Design of Fillet Welds in RHS-to-RHS Moment T-Connections under Branch In-Plane Bending

Mojgan Yaghoubshahi[a], Min Sun[a,*] and Kyle Tousignant[b]

[a] Department of Civil Engineering, University of Victoria, Victoria, BC, V8P 5C2, Canada

[b] Department of Civil & Resource Engineering, Dalhousie University, Halifax, NS, B3H 4R2, Canada

[*] Corresponding Author. E-mail: msun@uvic.ca

Abstract

Non-linear finite element (FE) models were developed to assess the AISC 360-16 Chapter K design approach for fillet welds in rectangular hollow section (RHS) moment T-connections under branch in-plane bending. The FE models were validated by comparison of the weld fracture moments, load-deflection responses, and spot-strain measurements to results from six previous, large-scale, weld-critical experiments. Based on all available experimental and FE data, the AISC 360-16 design approach is shown to be over-conservative. A key reason for this is that it does not account for bearing between the branch and chord on the compression side of the connection. New design formulae that take bearing into account are hence proposed. These formulae are shown to provide more accurate predictions of fillet weld strength in RHS moment T-connections under branch in-plane bending, and yet still achieve a safety (reliability) index that meets the AISC's target value of 4.0 for connections. The scope of this paper covers connections with all-around fillet welds and branch-to-chord width ratios up to 0.85.

Keywords

Rectangular hollow sections, Fillet welds, Effective properties, Moment connections, Parametric study, Finite element analysis

1. Introduction

For welds in hollow structural section (HSS) connections, contemporary standards and guides [1-4] acknowledge two design methods: (1) design of the weld to develop the yield strength of the connected branch member wall, or (2) design of the weld to resist the actual forces in the connected branch member. Method 1 is an upper-bound approach that permits a prequalified weld size to be easily determined; however, in many situations it is over-conservative. Method 2 generally allows downsizing of the welds, which is desirable because it can lower the fabrication cost of the connection. Method 2 (the so-called “fit-for-purpose” approach) provides the most benefit when branch member forces are low relative to their capacity.

With Method 2, designers are required to use weld effective properties (i.e. weld effective lengths and weld effective section moduli) that take into account the non-uniform loading of the weld perimeter due to variations in the local stiffness of the welded chord face normal to its surface. (With Method 1, this phenomenon is “automatically” considered.) Weld effective properties have been researched and recommended for rectangular hollow section (RHS) connections including axially-loaded T-, Y-, and X-connections, gapped and overlapped K-connections, and moment-loaded T-connections [5-13]. These recommendations form the basis of a comprehensive “weld effective length” design method given in Section K5 of AISC 360-16 [4] (the American steel code) that covers a broad range of RHS connection types and loadings. Research has also been conducted recently on the non-uniform loading of welds in circular hollow section (CHS) connections [10,12,14-16].

Since Section K5 was first introduced (as Section K4, in AISC 360-10 [17]), the design approach for welds in RHS-to-RHS moment T-connections under branch in-plane bending has seen little scrutiny. McFadden and Packer [13] found it to be over-conservative (yet safe); however, their recommendation, which was to liberalize the formula for the weld effective elastic section modulus, was limited by their sample size (10 weld-critical connections). This paper presents a finite element (FE) study to: (i) extend the database of weld-critical tests on RHS-to-RHS moment T-connections under branch in-plane bending; and (ii) develop a better (more accurate, yet still safe) formula for the nominal weld strength in connections with all-around fillet-welds (i.e. $\beta \leq 0.85$).

2. Background

AISC 360-16 Section K5 gives design formulae to determine the nominal flexural strength of welds in RHS-to-RHS moment connections ($M_{n\text{-}ip}$ for in-plane bending and $M_{n\text{-}op}$ for out-of-plane bending) based on Method 2, the fit-for-purpose approach. These formulae consider the sole limit state of shear rupture through the plane of the weld effective throat (t_w) as the governing failure mode. In Section K5, the nominal flexural strength of the weld around the perimeter of the RHS branch is computed as the product of the nominal weld stress (F_{nw}) and the weld effective elastic section modulus (S_{ip} for in-plane bending and S_{op} for out-of-plane bending). F_{nw} is specified in AISC 360-16 Table J2.5 as 0.60 times the minimum tensile strength of the weld metal (F_{EXX}) for both fillet welds and partial joint penetration (PJP) groove welds. $M_{n\text{-}ip}$ and $M_{n\text{-}op}$ are hence:

$$\mathrm{M_{n-ip}} = \mathrm{F_{nw}S_{ip}} = 0.60\mathrm{F_{EXX}S_{ip}} \tag{1a}$$

$$\mathrm{M_{n-op}} = \mathrm{F_{nw}S_{op}} = 0.60\mathrm{F_{EXX}S_{op}} \tag{1b}$$

To calculate the design strength of the weld, a resistance factor (ϕ_w) of 0.75 or 0.80 is applied to Eqs. (1a) and (1b) for fillet welds and PJP groove welds, respectively. The AISC 360-16 Chapter K equations for S_{ip} and S_{op} in RHS-to-RHS T-, Y- and X- (or cross-) connections under branch bending are given in Table 1.

Table 1. Effective elastic section moduli for RHS T-, Y- and X- (or cross-) connections under branch bending (adapted from [4])

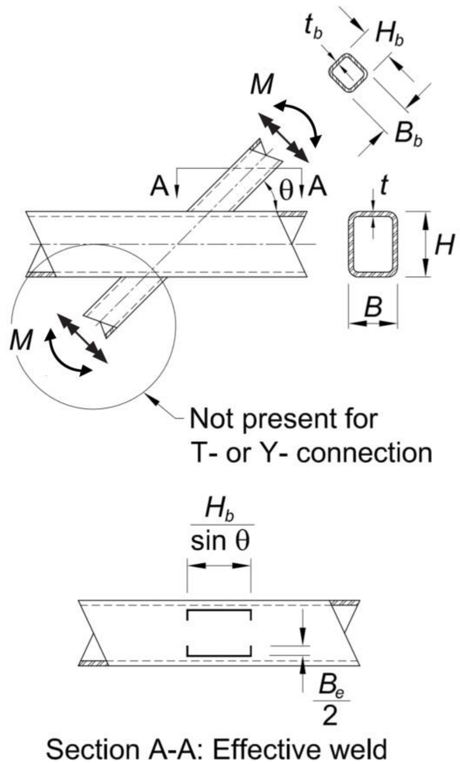	$S_{ip} = \frac{t_w}{3}\left(\frac{H_b}{\sin\theta}\right)^2 + t_w B_e\left(\frac{H_b}{\sin\theta}\right)$ (2a) $S_{op} = t_w\left(\frac{H_b}{\sin\theta}\right)B_b + \frac{t_w}{3}\left(B_b{}^2\right) - \frac{(t_w/3)(B_b - B_e)^3}{B_b}$ (2b) where $B_e = \left(\frac{10t}{B}\right)\left(\frac{F_y t}{F_{yb} t_b}\right) B_b \leq B_b$ (2c) when $\beta > 0.85$ or $\theta > 50°$, $B_e/2$ shall not exceed $B_b/4$.

Eqs. (2a) and (2b) in Table 1 are derived by Packer and Sun [8]. These equations are based on elastic theory and assume that only a portion of the length of the two transverse weld elements (located along the branch width, B_b) is effective. Eq. (2c) gives the effective length of each of these elements (B_e) and is based on previous research on non-uniform loading in transverse plate-to-RHS connections [18].

McFadden and Packer [13] tested 12 RHS-to-RHS T-connections under branch in-plane bending to determine the effectiveness of the welded joint. Two of the 12 specimens failed by punching shear of the connected chord face (which is considered a "connection failure"). The remaining 10 specimens failed by weld rupture. Test data from the 10 "weld-critical" tests was used to evaluate the AISC 360-10 [17] design approach, which was found to be over-conservative. It was hence recommended to change the notwithstanding clause "when $\beta > 0.85$ or $\theta > 50°$, $B_e/2$ shall not exceed 2t" (in AISC 360-10) to "when β > 0.85 or θ > 50°, $B_e/2$ shall not exceed $B_b/4$" (as shown in Table 1) for all RHS-to-RHS T-, Y- and X-connections under branch in-plane bending and under branch axial load. This recommendation was adopted in AISC 360-16.

Fig. 1 illustrates the relationship between the actual weld rupture moment (M_a) under branch in-plane bending and M_{n-ip} according to AISC 360-16 (i.e. M_{n-ip} calculated using Eq. (1a) and Table 1 with the measured values of F_{EXX}, t_w, B_b, H_b, t_b, B, H, and t reported by [13]) for the 10 weld-critical tests [13]. As shown in Fig. 1, the mean ratio of actual-to-predicted strength (m_R) is 2.19. The actual-to-predicted ratio for each specimen ranged from 1.34 to 4.04. This ratio is quite high, indicating that the AISC 360-16 design approach using Eq. (1a) and Table 1 may still be over-conservative.

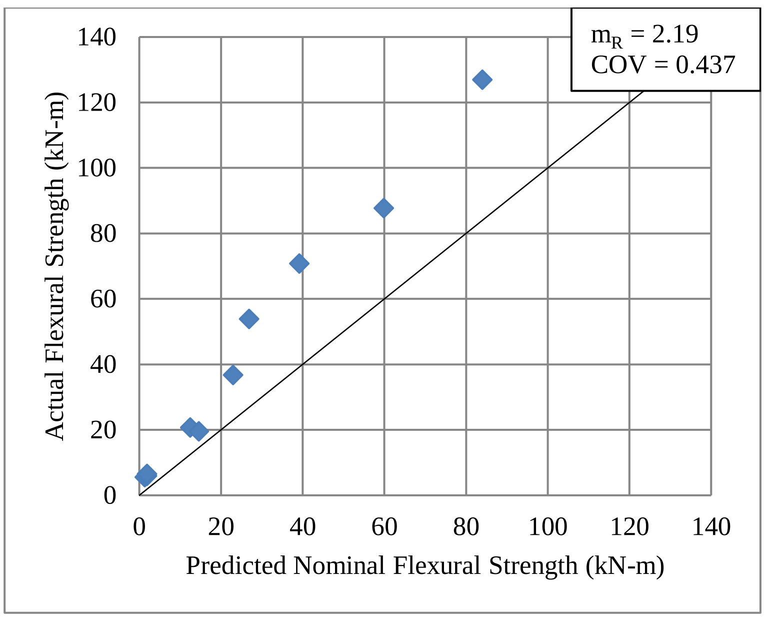

Fig. 1. Actual versus predicted nominal flexural strengths according to AISC 360-16 (adapted from [13])

3. Finite element modelling

To evaluate the AISC 360-16 design approach using Eq. (1a) and Table 1 over a wider range of parameters, the previous results by [13] were extended using FE modelling. For initial validation of the FE models, the geometric and mechanical properties of the sections and materials reported by

McFadden and Packer [13] for six connection specimens were used to develop replicate FE models in ABAQUS [19]. The measured dimensions of the RHS sections (H, B, t, H_b, B_b, and t_b as shown in Table 1) and the weld throat dimension (t_w) for each specimen are listed in Table 2. All connections listed have $\beta < 0.85$.

Table 2. Geometric properties of six RHS connection specimens tested by McFadden and Packer [13]

Connection ID	θ (º)	RHS chord member $H \times B \times t$ (mm)	RHS branch member $H_b \times B_b \times t_b$ (mm)	β	B/t	τ	t_w (mm)
T-0.25-34	90	203.7 × 203.7 × 5.89	51.2 × 51.2 × 5.76	0.25	34	0.98	2.39
T-0.25-23	90	202.8 × 202.8 × 8.74	51.2 × 51.2 × 5.76	0.25	23	0.66	2.39
T-0.25-17	90	204.5 × 204.5 × 11.58	51.2 × 51.2 × 5.76	0.25	17	0.50	2.39
T-0.75-34	90	203.7 × 203.7 × 5.89	152.6 × 152.6 × 5.74	0.75	34	0.97	2.54
T-0.75-23	90	202.8 × 202.8 × 8.74	152.4 × 152.4 × 8.69	0.75	23	0.99	3.30
T-0.75-17	90	204.5 × 204.5 × 11.58	152.6 × 152.6 × 11.67	0.75	17	1.01	5.59

In Table 2, each “Connection ID” is consistent with [13] and includes two numbers: the first number is the branch-to-chord width ratio of the connection ($\beta = B_b/B$), equal to 0.25 of 0.75; the second number is the chord width-to-thickness ratio ($2\gamma = B/t$), which ranges from 17 to 34. The connections also cover a wide range of branch-to-chord thickness ratios ($\tau = t_b/t$) from 0.50 to 1.01.

The FE boundary conditions for the models were chosen to simulate the test setup used by McFadden and Packer [13], which is shown in Fig. 2. It should be noted that the “point load device” (see Fig. 2) ensured that the applied load remained horizontal and in plane throughout each test. It can therefore be assumed that the moment arm (i.e. the vertical distance from the load application point to the welded joint) was constant as the branch deflected.

To measure branch deflection, and determine the applied moment, McFadden and Packer [13] used an optical camera to record the coordinates of strobing light emitting diode (LED) targets (see Fig. 3 for locations) and cross-multiplied the vector of the applied load with a position vector drawn through these coordinates. Fig. 4 shows the branch deflection profile at different load levels for a typical connection (based on data from the LED targets), in which the vertical movements of all LED targets is shown to be negligible. This gives further credence to the assumption of a constant moment arm.

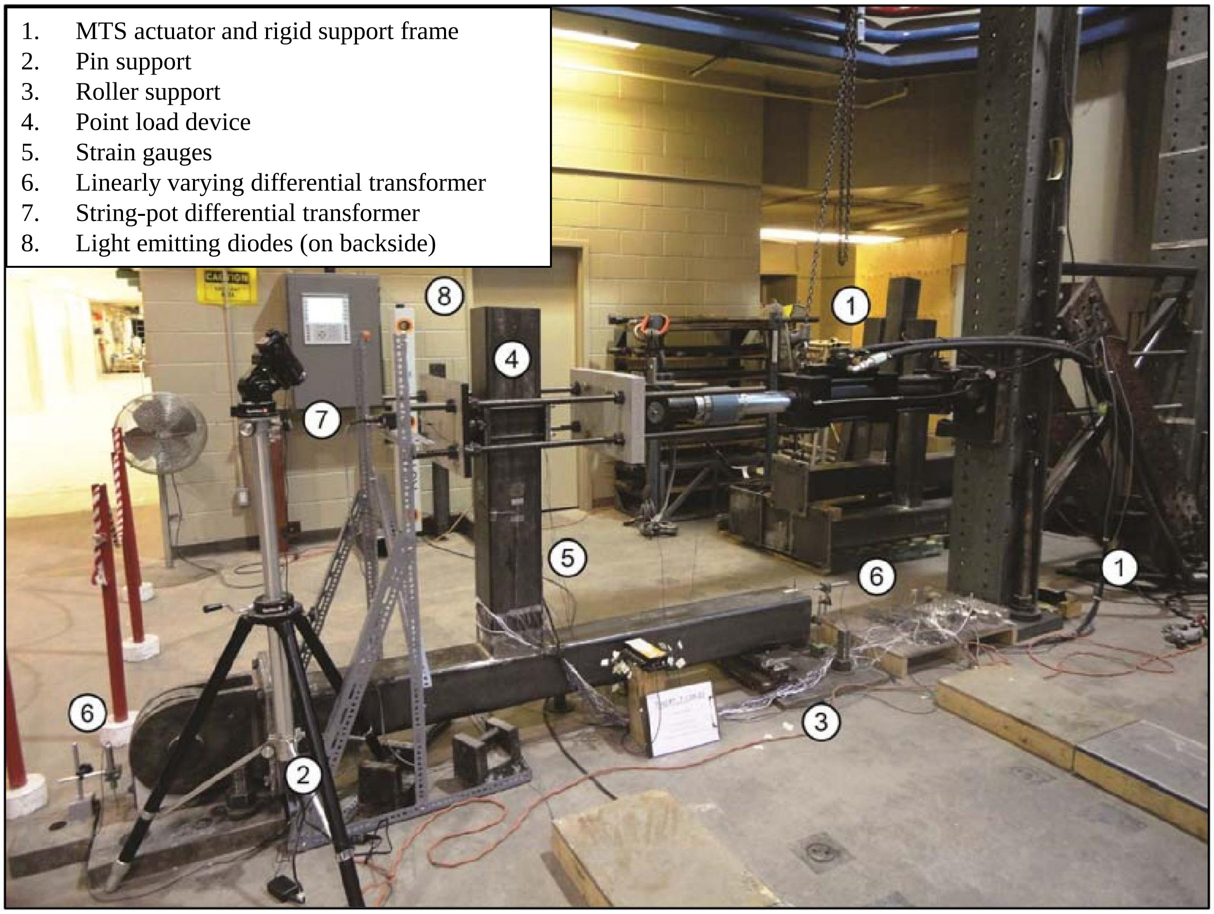

Fig. 2. RHS-to-RHS moment T-connection experimental test setup [13]

Fig. 3. Typical LED target locations [13]

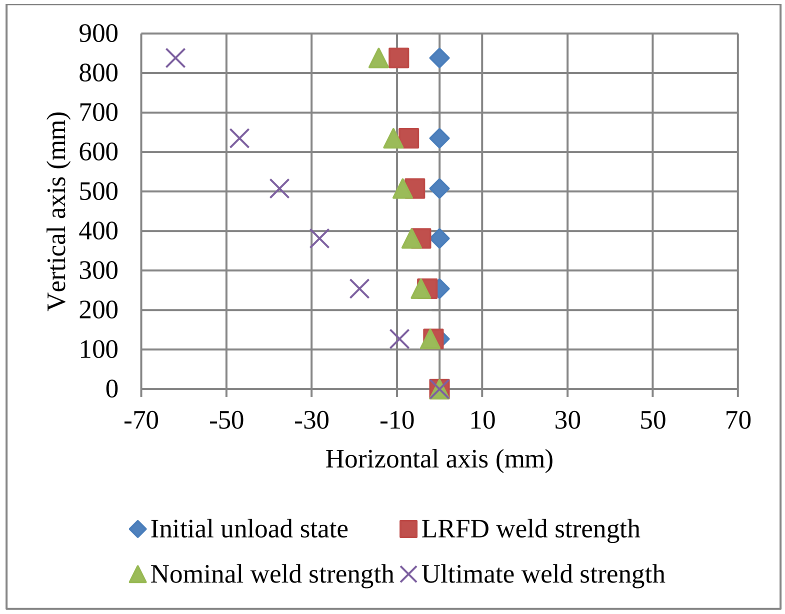

Fig. 4. Typical branch deflection profiles at different load levels based on data from LED targets [13]

3.1 Material properties

The experimental program reported by McFadden and Packer [13] included tensile coupon (TC) tests on both the RHS base metal (i.e. the chord and branch members) and the as-laid weld metal. Because this information was readily available, it has been used herein to model the respective materials in the FE analyses. The procedure used to convert the experimental engineering stress (σ) and engineering strain (ε) ordinates (reported by [13]) to true stress (σ_T) and true strain (ε_T) ordinates (required by the FE program) is consistent with previous research [12,15,20,21]. Prior to necking, Eqs. (3a) and (3b) were used:

$$\sigma_T = \sigma(1 + \varepsilon) \tag{3a}$$

$$\varepsilon_T = \ln(1 + \varepsilon) \tag{3b}$$

After necking, Eq. (4), developed by Ling [22], which relies on an iterative method involving FE modelling of the experimental TCs directly, was used:

$$\sigma_T = \sigma'_T \left[w(1 + \varepsilon_T - \varepsilon'_T) + (1 - w) \left(\frac{\varepsilon_T^{\varepsilon'_T}}{\varepsilon_T'^{\varepsilon'_T}} \right) \right] \tag{4}$$

where σ'$_T$ = true stress at the start of necking, ε'$_T$ = true strain at the start of necking, and w = weighting factor.

Eq. (4) is necessary to model the post-necking σ_T – ε_T response because the stress distribution at the point of necking changes from a simple uniaxial case, represented by Eqs. (3a) and (3b), to a more complex triaxial case [23]. Using Eq. (4), w for each different material (i.e. the RHS branch and chord members, and the weld metal) were be determined by matching the post-necking σ – ε curve of a TC modelled in ABAQUS to one obtained experimentally for the same material. A comparison of several typical FE and experimental σ – ε curves and the corresponding σ_T – ε_T curves obtained in this manner are shown in Fig. 5. It should be noted that the ends of the experimentally obtained engineering σ – ε curves in Fig. 5 do not correspond to ruptures of the tensile coupons. During testing, the clip gauge was removed shortly after necking (i.e. at the end of the curves) to prevent damage to it. Average rupture strains of 30.0% and 28.5% were reported for the RHS material and the as-laid weld material, respectively [13].

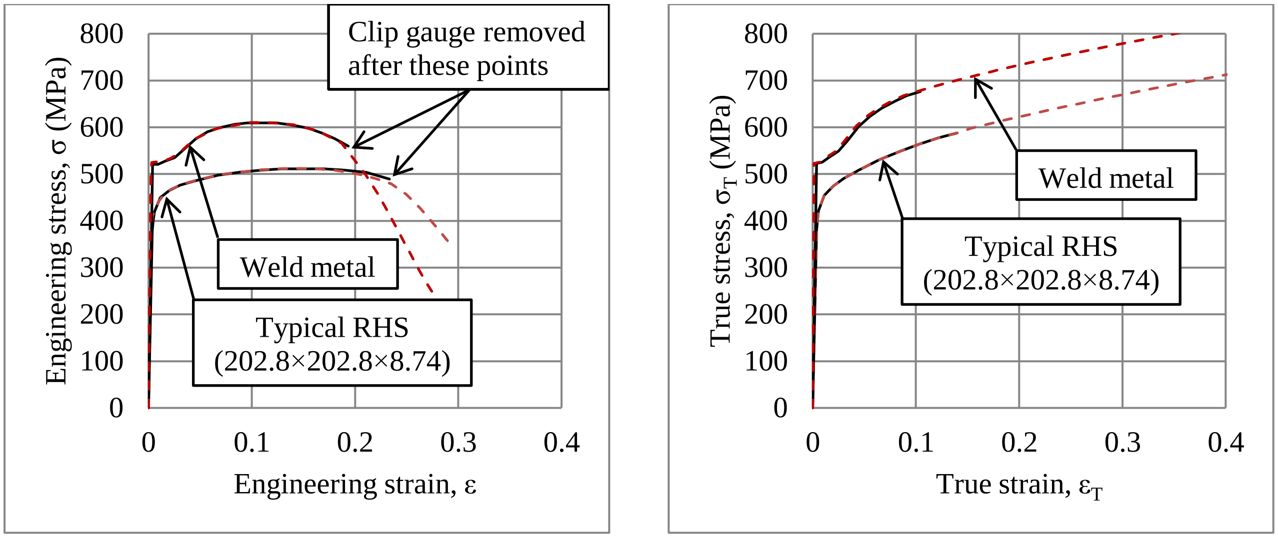

(a) Engineering stress-strain (b) True stress-strain

Fig. 5. Comparison of typical experimental (solid line) and FE (dashed line) stress-strain curves

3.2 Connection modelling

A typical FE model of an RHS-to-RHS moment T-connection (i.e. one used in the current study) is depicted in Fig. 6. As shown, only half of each connection was modelled due to symmetry about a principal plane passing through mid-width of the RHS members. A symmetry boundary condition was hence applied along the “cut” face, as highlighted in Fig. 6. To model the discontinuity between the branch end and the chord surface, a "seam" feature was used (see Fig. 6). In the first time-step of the FE analysis, a “self-contact interaction”, with normal and tangential frictionless properties, was defined on the branch end and the chord surface at the seam. This prevented penetration of the branch elements into the chord elements on the compression side of the connection, and simulated the potential bearing of the branch end on the chord.

A sensitivity analysis determined that 8-noded linear brick element (C3D8R elements in ABAQUS, with three translational degrees of freedom per node and reduced integration formulation), with four elements through the branch and chord thickness, provided convergent initial stiffness and load-deformation responses for all six connections. The mesh pattern used with these parameters is illustrated

Fig. 6. Based on the same sensitivity analysis, the length of all sides of any brick element at the joint location were forced to be no larger than 1.27 mm. Away from the joint, larger elements were used, with a biased mesh pattern ensuring a smooth transition between the areas of fine and coarse mesh (as shown in Fig. 6).

To simulate the pin and roller used by [13] (Fig. 2), first, a rigid body constraint was defined for each chord end. This constraint was used to slave all nodes on each end to a single reference point (RP) located in the centre of the cross section on the same end (see “RPs” Fig 6). Then, restraint conditions were applied to the RPs. For the pin (RP3 in Fig. 6), all translational degrees of freedom were restrained for the RP; for the roller (RP2 in Fig. 6), only the two translational degrees of freedom perpendicular to the longitudinal axis of the chord member were restrained.

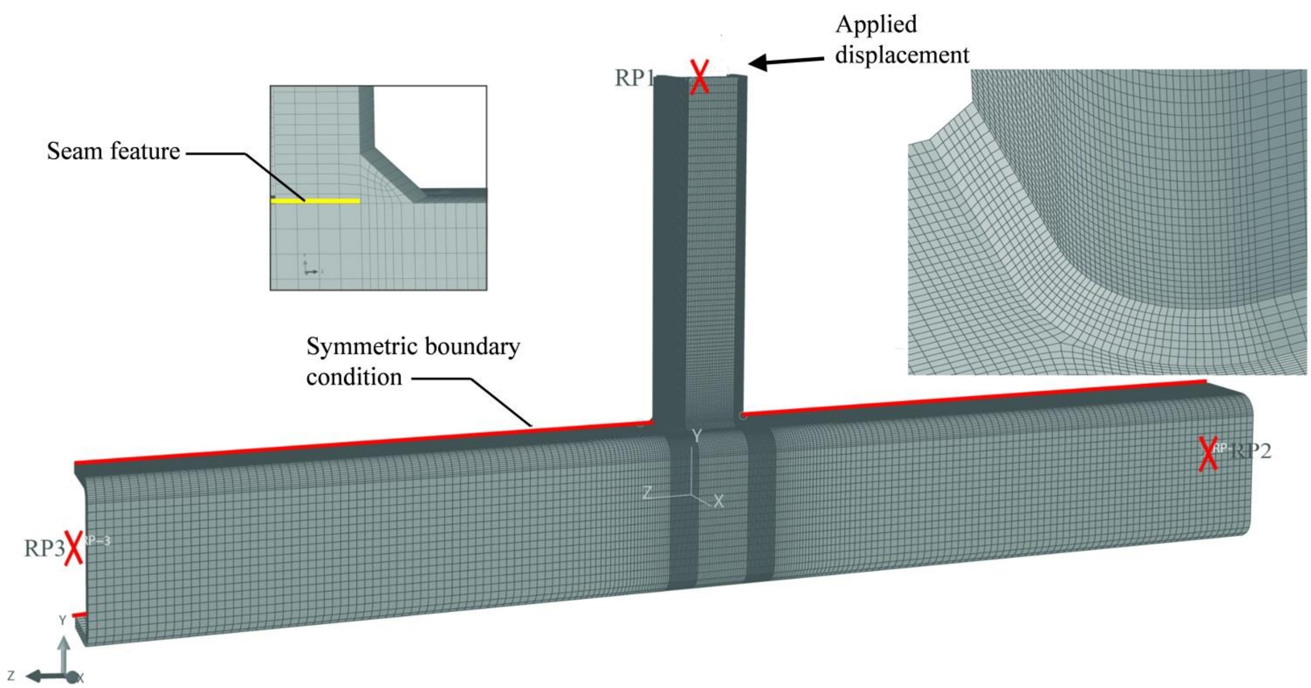

Fig. 6. Typical FE RHS-to-RHS moment T-connection geometry, mesh layout, and boundary conditions

3.3 Initial comparison of experimental and FE results

Fig. 7 shows the experimental and FE moment-deflection curves for the six tests chosen for validation. For all six tests, moment was calculated as the height measured from the connection, taken as the vertical distance from the top face of the chord (i.e. the plane containing the weld group at the un-deformed state) to the line of action of the horizontally applied load, multiplied by the applied load. The branch in-plane deflection for each specimen in Fig. 7 was measured horizontally at the load application point. It is shown that all FE moment-deflection curves agree reasonably well with the experimental curves up to weld fracture.

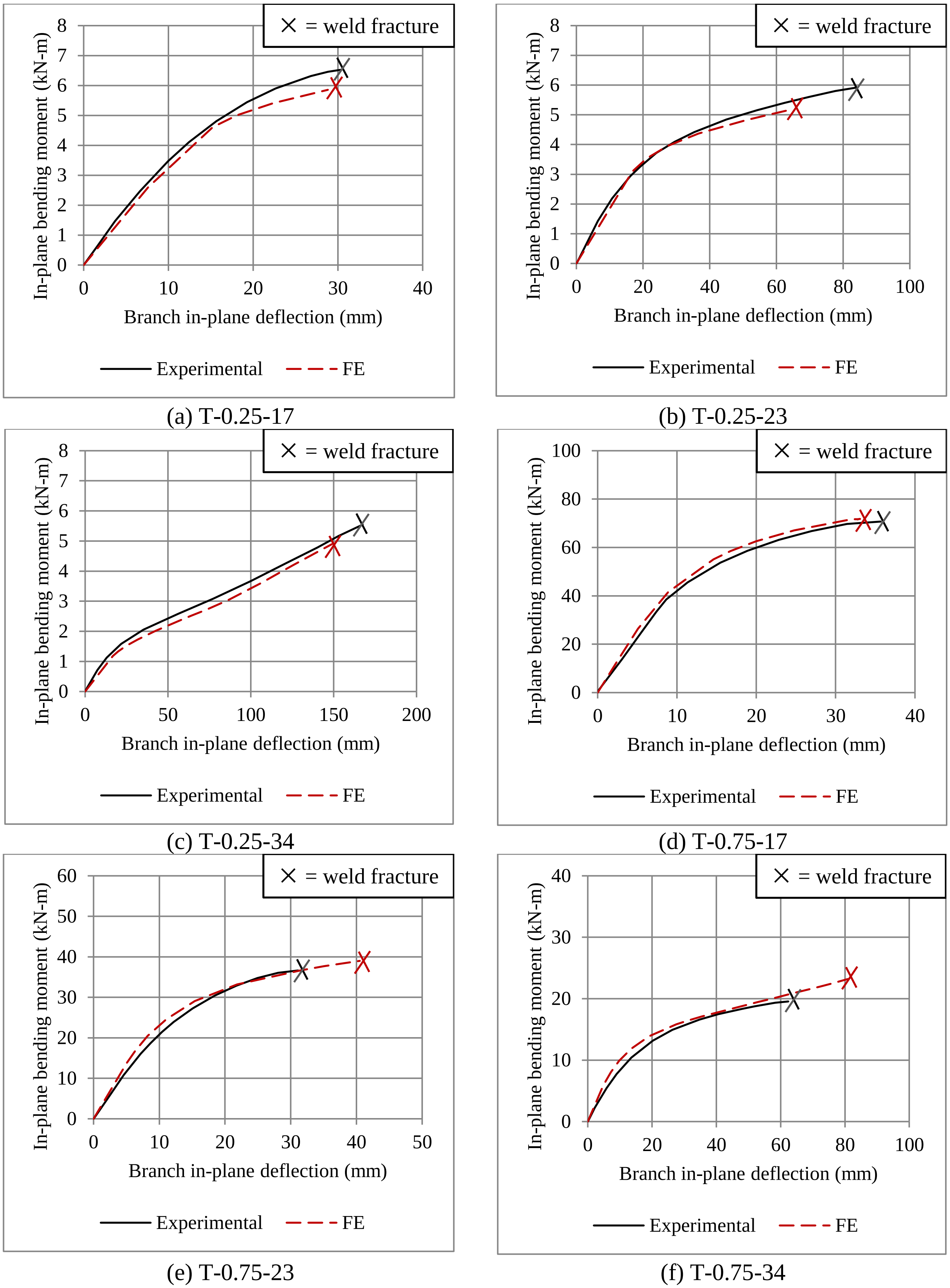

Fig. 7. Comparison of experimental and FE moment-deflection curves

3.4 Weld fracture criterion

For determination of the weld fracture moment (i.e. the ultimate moment for weld-critical connections), an FE fracture criterion based on equivalent (von Mises) strain was used. This concept was also used by [12,15,20,21] on similar research topics. The method assumes that when the von Mises strain in an element reaches a critical value (ε_{ef} = equivalent strain at rupture), the stiffness and the stress of that element are reduced to near zero, to model the effect of fracture. The applied load is then transferred to adjacent elements where the equivalent strain is still lower than ε_{ef}. With increased loading, the stiffness and the stress of the adjacent elements will also be reduced to near zero values (once the von Mises strain reaches ε_{ef}) simulating crack propagation.

In the previous research [12,15,20,21], the above approach to simulate fracture was programmed in ANSYS using the element "death feature". In the current research, the approach was programed in ABAQUS, by adopting a method described in the "Damage and Failure for Ductile Metals" chapter of the ABAQUS Analysis User's Guide [19]. This method assumes a typical σ_T – ε_T material response, shown in Fig. 8, which includes: (1) undamaged constitutive behaviour (e.g. elastic-plastic with hardening); (2) damage initiation (point A); (3) damage evolution (path A – B); (4) choice of element death/deactivation (point B). This method is empirical since experimental data is needed to determine the values for points A and B. Following the "element death" concept used by [12,15,20,21], this study used a damaged response following path A to B'. In other words, instead of a gradual stiffness reduction, this study assumed that the stiffness and the stress of an element is reduced to near zero values when the von Mises strain reaches the strain value ε_T at A, which is defined as the equivalent strain at rupture (ε_{ef}).

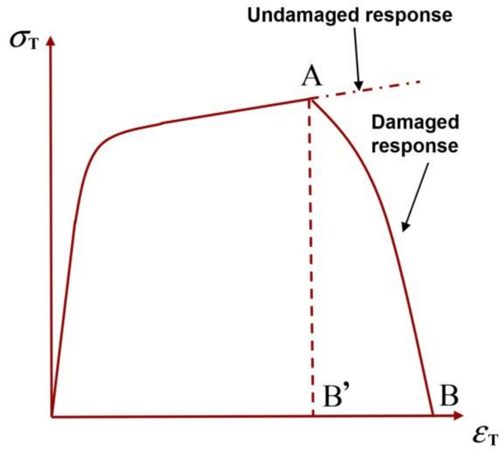

Fig. 8. Typical material response showing progressive damage [19]

Following the method used by [12,15,20,21], the ε_{ef} value was determined by comparison of the experimental and numerical ultimate moments and ultimate deflections for all six connection specimens in Fig. 7. A trial-and-error approach was adopted to determine the best-fit ε_{ef} value that minimized the difference between the experimental and FE results for these two parameters. An average best-fit ε_{ef} value of 0.25 was eventually selected as the fracture criterion for the parametric study. As can be seen in Fig. 7, for both the maximum branch in-plane deflections and the ultimate weld strengths, the finite element simulations agree reasonably well with the experimental results for all six connections. Comparing the numerical values of actual-to-predicted fracture load and displacement for all six connections in Fig. 7, ε_{ef} = 0.25 results in an average value (and coefficient of variation, COV) of 1.03 (0.12) and 1.02 (0.21), respectively, indicating acceptable agreement.

3.5 Further comparison of experimental and FE results

During experimental testing, McFadden and Packer [13] used linear strain gauges (see Fig. 9) to measure the non-uniform distribution of normal strain around the branch footprint. The strain gauges were oriented along the longitudinal axis of the branch and placed approximately 15 mm above the weld toe to avoid the high strain region immediately adjacent to the weld caused by the notch effect [7].

Theoretically, under pure in-plane bending moment, the distribution of strain around the branch footprint on both sides of the branch and chord longitudinal centerline is symmetric. Hence, strain gages were installed only around half the branch perimeter. An additional gage was placed at the theoretical zero stress region on the opposite longitudinal mid-wall of the branch to monitor any significant out-of-plane effects throughout testing.

Fig. 9. Strain gauges adjacent to the welded joint for determination of uneven strain distribution in the branch longitudinal direction [13]

For further validation of the FE models, the experimentally obtained strain gauge data at different load levels was compared to the FE strains at the same locations, for all six connections. Typical comparisons are shown in Fig. 10. When the applied load approaches the nominal weld strength ($M_{n\text{-}ip}$) according to AISC 360-16, calculated using Eq. (1a) and the formulae in Table 1, good agreement between the experimentally measured and numerically obtained strains is obtained. In contrast, at the ultimate moment, some of the FE strain values deviate significantly from the experimental results. This occurs due to progressive and non-uniform yielding of the weld along its length, due to variations in the experimental weld geometry. These variations were not captured in the FE models.

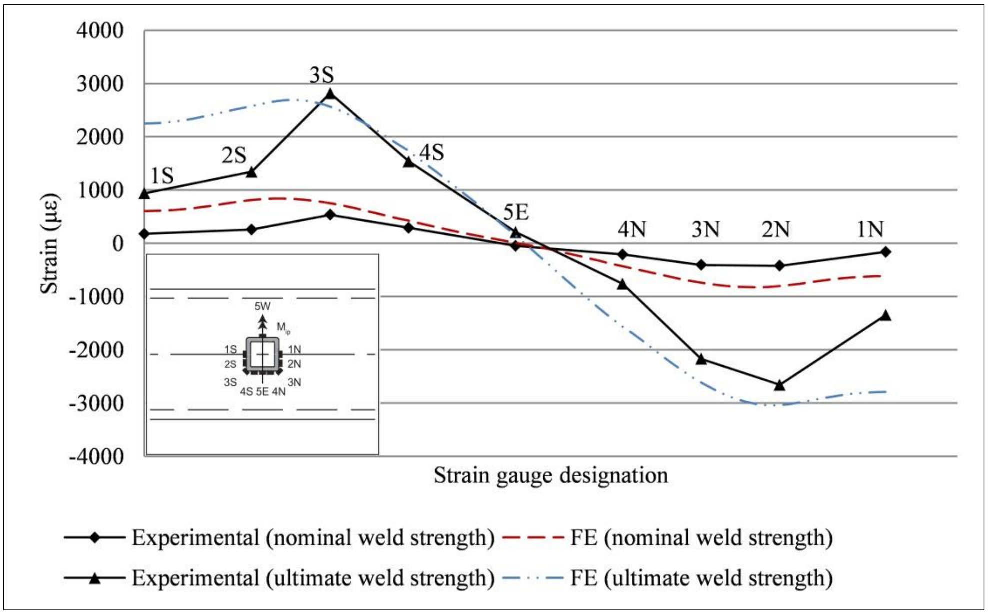

(a) T-0.25-34

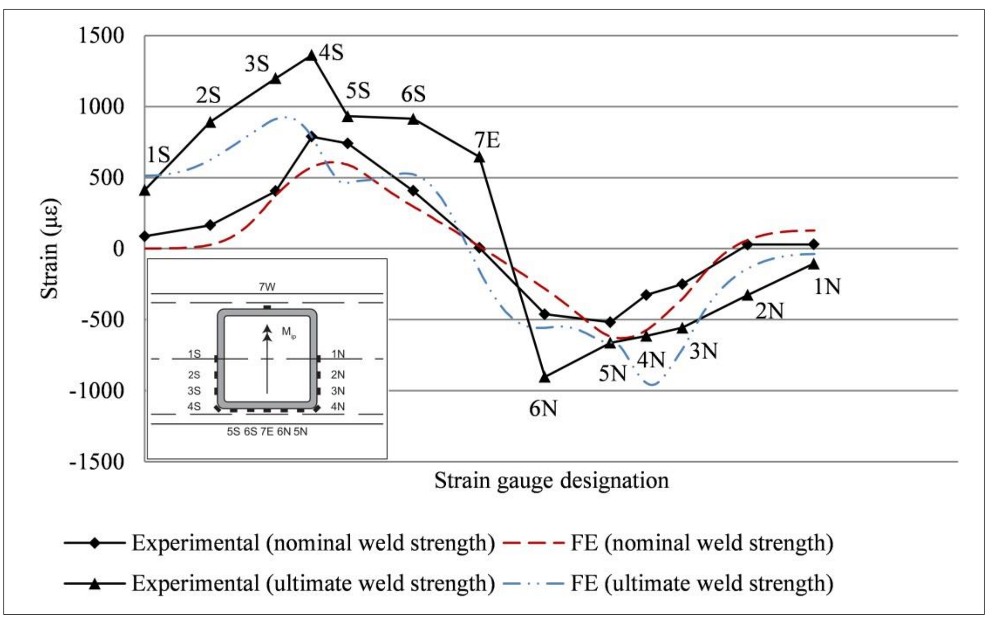

(b) T-0.75-23

Fig. 10. Comparison of typical experimental and FE longitudinal strain distribution adjacent to the weld at different load levels (nominal and ultimate weld strengths)

Fig. 11 shows a comparison of the typical location of crack initiation in the experimental and FE joints. Both Figs. 10 and 11 capture the general phenomenon of high stress concentration and crack initiation at the corner region on the tension side of the welded joint. Hence, further credence is given to the accuracy of the FE models developed in Section 3.2.

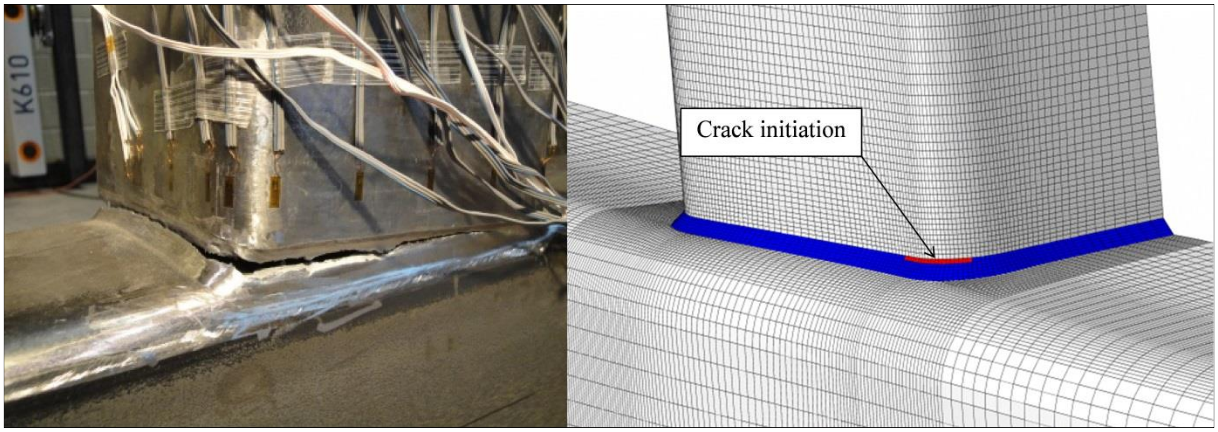

Fig. 11. Typical location of crack initiation in welded joints

4. Numerical parametric study

4.1 Effect of model size (scalability)

Prior to determination of the scope of the subsequent parametric study in Section 4.3, the scalability of the FE models and the fracture criterion developed in the previous sections were evaluated. The evaluation was performed using the method suggested by [15]. The same non-dimensional parameters (including β, B/t, and τ), but different absolute geometric dimensions, were modelled. Table 3 compares the actual weld rupture moments (M_a) from the FE analyses to the predicted nominal flexural strengths ($M_{n\text{-}ip}$) calculated using the formulae in Table 1. Same as the observations by [15], it was found that structural response (strength and defection) as well as the fracture criterion developed herein were in general the same for models with the same non-dimensional parameters.

Table 3. Effect of model size

B_b and H_b (mm)	β	B / t	τ	t_w / t_b	M_a / $M_{n\text{-}ip}$
200	0.5	17	0.7	0.3	1.39
100					1.38
50					1.38
25					1.36

4.2 Ranges of parameters

A range of non-dimensional key parameters was chosen to create all possible θ = 90° square RHS-to-RHS moment T-connections for the parametric study. The parameters varied were: B/t =15, 25, and 35, β = 0.25, 0.35, 0.45, 0.55, 0.65, 0.75, and 0.85, and τ = 0.2, 0.4, 0.6, 0.8, and 1. A total of 105 permutations exist for the values given; however, only 61 of them are possible in accordance with the AISC 360-16 [4] Table K.4.2A Limits of Applicability of Table K4.2 and the range of standard RHS sections available for designers in the AISC Manual [24]. Hence, only those 61 connection models have been analysed herein.

4.3 Details of parametric models

The chord member of all parametric models was 1600 mm in length (i.e greater than 6B to ensure that the connection was sufficiently far away from the support to mitigate the effects of end constraints on the stress distribution at the joint) and had a constant width of B = 203 mm. On the other hand, the branch members had various lengths (set as a function of the branch member width), but they were always longer than $3B_b$ to avoid "end effects" [15, 25]. The remaining model dimensions were calculated from the β, B/t and τ values for each specific model, and a constant weld throat dimension of $t_w = 0.35t_b$ was used (for all connections) to ensure that weld fracture occurred prior to overall branch member yielding.

A single set of material properties (for the branch member, chord member, and the weld) were used in each model, and these were based on TC tests conducted by McFadden and Packer [13]. The stress-strain curve for each material is shown in Fig. 12, and the key material properties are summarized in Table 4.

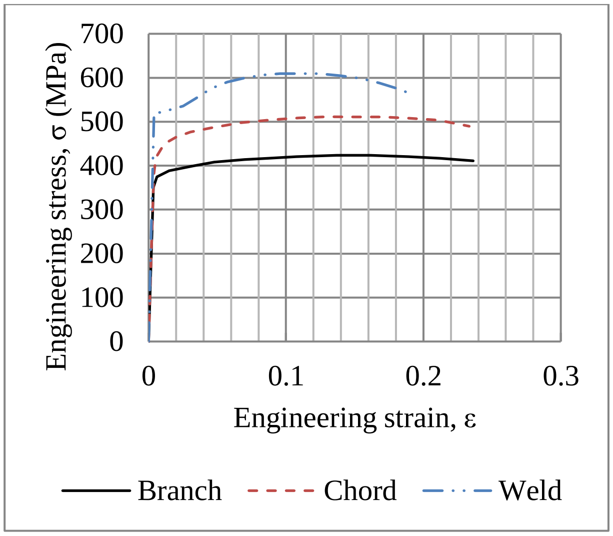

Fig. 12. Engineering stress-strain curves for materials used in parametric models

Table 4. Key material characteristics used in the parametric models

	E (MPa)	F_y (MPa)	F_u or F_{EXX} (MPa)
Chord	175,800	394	506
Branch	180,640	350	424
Weld	208,910	523	609

Based on equilibrium, for all parametric models, the in-plane bending moment at the welded joint location is calculated by multiplying the lateral force by the vertical distance between the line of application of the force/displacement and the top face of the chord (i.e. the plane containing the weld group at the un-deformed state).

5. Results and evaluation of parametric study

All FE connections failed by weld fracture. Using the geometric and material properties described in Section 4, Eq. (1), and the formulae in Table 1, the predicted nominal in-plane flexural strength of the welded joint ($M_{n\text{-}ip}$) was calculated for each FE connection. The predicted strengths are compared to the actual strengths (numerically obtained from the FE analysis) in Fig. 13, and the actual-to-predicted ratios ranged from 1.41 to 4.29. The average actual-to-predicted ratio (m_R) is 2.72 (COV = 0.274). Same as the observations by McFadden and Packer [13] (see Section 1), the predictions using the current AISC 360-16 Chapter K formulae are found to be very conservative.

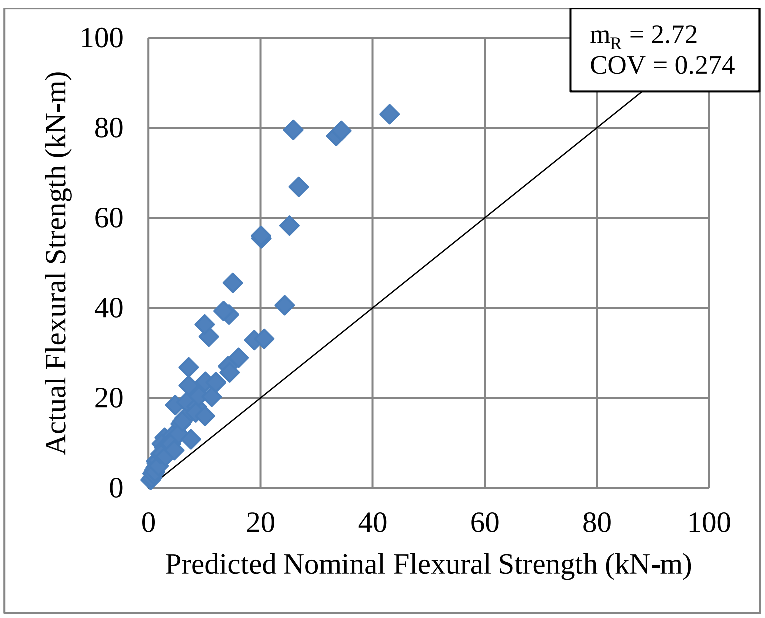

Fig. 13. FE versus predicted nominal flexural strengths using Eqs. 2a and 2c

Careful analysis of the FE data with respect to contact that occurred in the FE models indicated that the applied in-plane bending moment is transferred through both the weld and the branch wall, through bearing on the compression side of the connection. This bearing mechanism causes a shift of neutral axis location towards the compression side, and this phenomenon was observed in all the FE models at the ultimate load level (see Fig. 14 for an example).

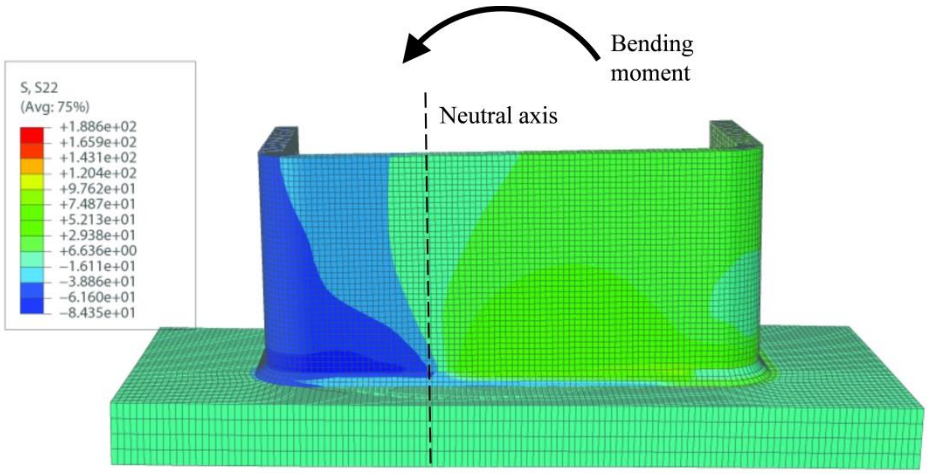

Fig. 14. Stress contour of RHS connection under branch in-plane bending (MPa)

Taking this bearing mechanism into account, B_e and the location of the neutral axis (y_t), measured from the tension side of the connection (see Fig. 15), can be calculated by solving a system of three equations of compatibility and equilibrium given in Eqs. (5a-c):

$$\frac{y_t}{H_b} = \frac{F_{nw}}{(F_{nw} + \sigma_c)} \tag{5a}$$

$$F_{nw}B_e t_w + F_{nw} y_t t_w = \sigma_c B_e (t_b + t_w) + \sigma_c (H_b - y_t)(t_b + t_w) \tag{5b}$$

$$M_{n-ip} = F_{nw}B_e t_w y_t + \frac{2}{3}F_{nw}{y_t}^2 t_w + \sigma_c B_e (t_b + t_w)(B_b - y_t) + \frac{2}{3}\sigma_c (t_b + t_w)(H_b - y_t)^2 \tag{5c}$$

where σ_c = maximum compressive stress (on the side of the connection where weld rupture does not occur).

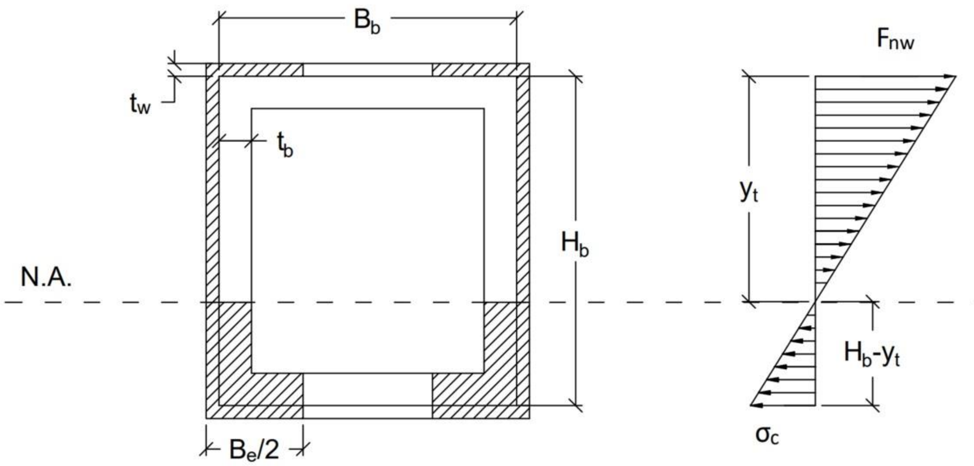

Fig. 15. Connection bending plan and stress distribution on weld and branch wall

Eqs. (5a-c) assume that a uniform stress occurs over the effective width(s) (B_e) of the transverse elements (i.e. they ignore the thickness of the weld and branch wall in determining the stress acting on them), and that “plane sections remain plane”. For simplicity, Eqs. (5a-c) also omit the RHS corner radii. By setting Eq. (5c) equal to the weld rupture moment M_a from the FE analyses or experiments, with F_{nw} taken as the nominal weld strength (= $0.60F_{EXX}$ for fillet welds, per Table J2.5 of AISC 360-16 [4]), the unknowns σ_c, y_t and B_e can be determined at the ultimate load.

In doing so, the location of the neutral axis measured from the tension side of the connection (“y_t”, in Fig. 15) can be shown to occur at a near-constant fraction of 0.75 times the branch member height (H_b). (For all FE connections, the ratio of y_t/H_b ranged from 0.72 to 0.77, with a COV of 0.020, or 2%.)

The resulting values of the effective width (B_e) can be normalized (by dividing by the branch width, B_b) and plotted against key connection parameters (i.e. B/t and τ), as shown in Figs. 16a and 16b. The points plotted in the figures are mean values with ± one standard deviation bars. In Figs. 16a and 16b, it is shown that the ratio B_e/B_b decreases as both B/t and τ increase, in agreement with Eq. (2c). If Eq. (2c) is normalized in the same manner as the FE data, it can be plotted in Figs. 16a and 16b. This has been done for typical end-range values of τ = 0.4 and 1.0 (see Fig. 16a) and B/t = 15 and 25 (see Fig 16b) without applying the limit of $B_e \leq B_b$. The notwithstanding clause (i.e. "when $\theta > 50^o$, $B_e/2$ shall not exceed $B_b/4$") in Table 1 has also been omitted. It can then be seen, in both figures, that the current AISC 360-16 effective width equation [Eq. (2c)] predicts the trend of the data well. But when B_e is calculated from Eqs. (5a-c) with $F_{nw} = 0.60F_{EXX}$, it is quite conservative.

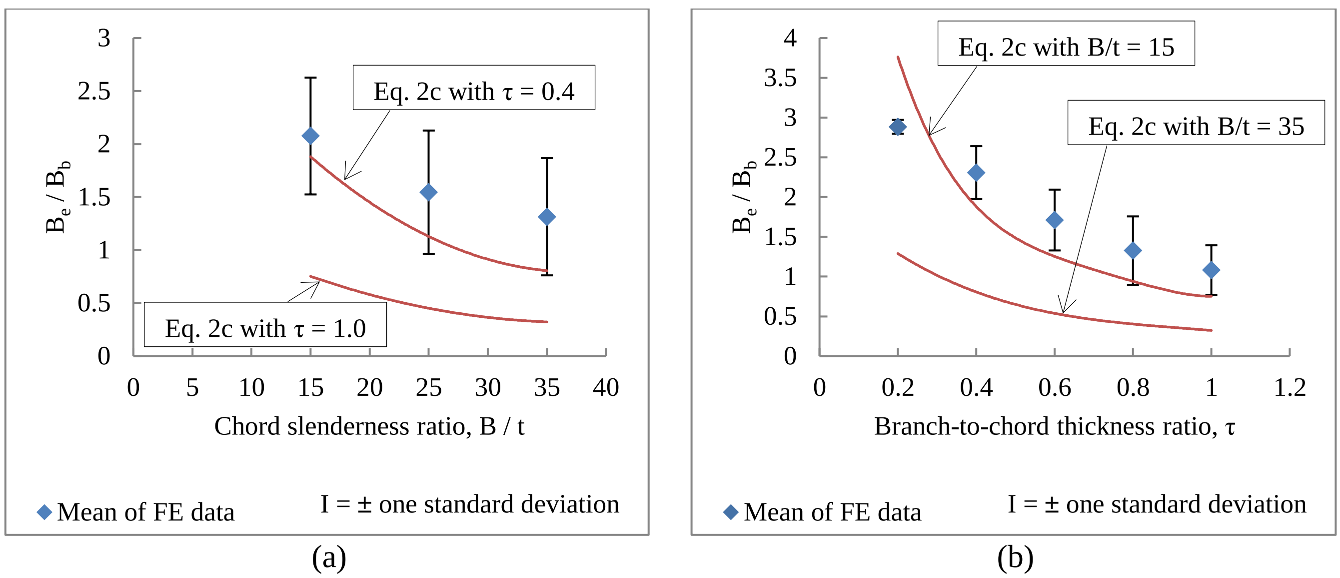

Fig. 16. Effect of (a) chord slenderness ratio and (b) branch-to-chord thickness ratio on effective length of transverse weld (with $F_{nw} = 0.60F_{EXX}$)

Tousignant and Packer [12] have shown that $F_{nw} = 0.60F_{EXX}$ is generally a conservative assumption for the nominal strength of fillet welds to the end of an RHS member. Furthermore, in RHS branch member connections, F_{nw} has been found to vary with the branch slenderness (B_b/t_b) and the ratio of the weld size to the branch wall thickness (t_w/t_b). The authors [12] provided an empirical equation for the strength of fillet welds in axially-loaded RHS connections that can be rearranged to give the following, accurate, expression for F_{nw} for fillet welds to RHS:

$$F_{nw} = \left[0.954 - 0.00193\left(\frac{B_b}{t_b}\right) - 0.210\left(\frac{t_w}{t_b}\right)\right] F_{EXX} \quad (6)$$

A similar equation by [12] for fillet welds to CHS has been used by [16] to derive weld effective lengths for CHS-to-CHS T-, Y- and X-connections.

By setting Eq. (5c) equal to the weld rupture moment M_a from the FE analyses, but with F_{nw} equal to Eq. (6), the unknowns σ_c, y_t and B_e can be recalculated. If this is done, the ratio of y_t/H_b remains largely unchanged (it ranges from 0.70 to 0.76, with a COV of 2%). The resulting values of B_e/B_b in this case are plotted against B/t and τ in Figs. 17a and 17b. It can now be seen, in both figures, that the current AISC 360-16 effective width equation (Eq. 2c) predicts the trend of the data well and is accurate.

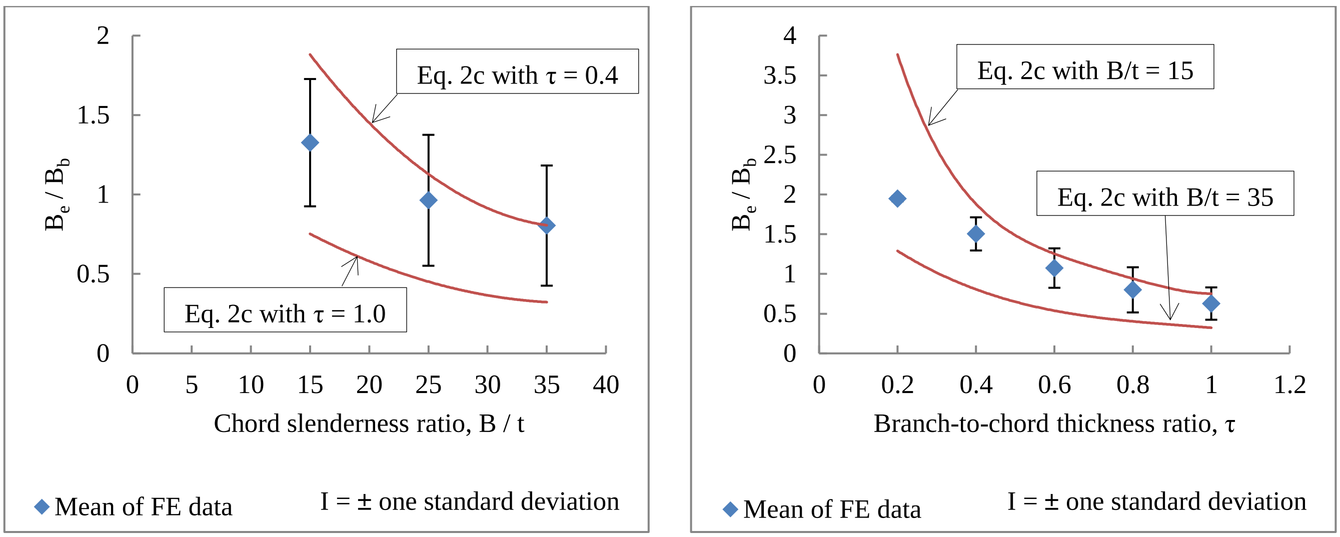

(a) (b)

Fig. 17. Effect of (a) chord slenderness ratio and (b) branch-to-chord thickness ratio on effective length of transverse weld with F_{nw} equal to Eq. (6)

It can therefore be concluded that the current AISC 360-16 [4] Chapter K formulae for the strength of fillet welds in RHS-to-RHS moment T-connections under branch in-plane bending are over-conservative for the following reasons:

(1) The direct bearing mechanism of load transfer between the branch and the chord on the compression side of the connection under in-plane bending is not considered in the S_{ip} formula in Table 1;

(2) The notwithstanding clause in Table 1 limiting the value of B_e (i.e. "when $\theta > 50^o$, B_e / 2 shall not exceed B_b / 4" in Table 1) is excessively conservative for connections under in-plane bending; and

(3) The assumed nominal stress of the fillet-weld metal ($F_{nw} = 0.60F_{EXX}$) is conservative for tension-loaded fillet welds to RHS.

6. Proposed Design Method

Based on the preceding evaluation, it is recommended to consider the location of the neutral axis in RHS-to-RHS moment T-connection subject to branch in-plane bending to be located at 3/4 of the branch footprint height from the tension side of the connection; i.e.:

$$y_t = \frac{3}{4}\frac{H_b}{\sin\theta} \tag{7}$$

The bearing mechanism on the compression side can be considered in calculating the joint capacity according to Eq. 1a by using a modified S_{ip} formula:

$$S_{ip} = \frac{1}{72}\left[(28t_w + t_b)\left(\frac{H_b}{\sin\theta}\right)^2\right] + \frac{1}{12}\left[(10t_w + t_b)B_e\left(\frac{H_b}{\sin\theta}\right)\right] \tag{8}$$

Eq. (8) was derived in the same manner as the Eq. (2a) in Table 1, using the procedure presented by Packer and Sun [8]. Moreover, Eq. (7) can be determined by deriving:

$$I_{ip} = \frac{1}{16}\left[\left(\frac{14}{3}t_w + \frac{1}{6}t_b\right)\left(\frac{H_b}{\sin\theta}\right)^3 + (10t_w + t_b)B_e\left(\frac{H_b}{\sin\theta}\right)^2\right] \tag{9}$$

and substituting into:

$$S_{ip} = \frac{I_{ip}}{y_t} = \frac{I_{ip}}{\left(\frac{3}{4}\frac{H_b}{\sin\theta}\right)} \tag{10}$$

in an analogous method to that used by Packer and Sun [8].

Using Eqs. (7-10), the maximum compressive stress (σ_c) will always be less than F_{nw} and the joint strength will be governed by weld rupture on the tension side of the connection.

Based on the analysis presented in Section 5 (Figs. 16a, 16b, 17a and 17b), it is recommended to use Eq. (2c) to determine B_e in Eq. (8) but to omit the notwithstanding clause (i.e. "when $\theta > 50°$, B_e / 2 shall not exceed B_b / 4" in Table 1). Finally, B_e must still be no greater than B_b, since this represents a physical limit.

7. Evaluation of proposed design method

7.1 Reliability analysis

To evaluate whether the current recommendation contains an adequate or excessive safety margin, a minimum safety index of $\beta^+ = 4.0$ (per Chapter B of the AISC 360-16 [4] commentary) was used to conduct a simplified reliability analysis. The resistance factor (ϕ_w) was calculated using the following formula suggested by [26,27]:

$$\phi_w = \phi_{\beta^+} m_R \exp\left(-\alpha\beta^+ \mathrm{COV}\right) \tag{11}$$

where m_R = mean of the ratio: (actual / predicted nominal strength = M_a / $M_{n\text{-}ip}$); COV = associated coefficient of variation of this ratio; α = coefficient of separation taken to be 0.55 [26,27]; β^+ = safety (reliability) index; and $\phi_{\beta+}$ = resistance modification factor when $\beta^+ \neq 3.0$ [27]. The formula for $\phi_{\beta+}$, was derived by Franchuk et al. [28]:

$$\phi_{\beta^+} = 0.0062(\beta^+)^2 - 0.131\beta^+ + 1.338 \tag{12}$$

The design method proposed in Section 5 was used to calculate the nominal strengths ($M_{n\text{-}ip}$) of: (1) the 61 welded joints investigated in the parametric study; and (2) the six connection specimens tested by McFadden and Packer [13] in Table 2 that failed by weld rupture, using three different methods for calculation of F_{nw}:

(i) $F_{nw} = 0.60F_{EXX}$ according to AISC 360-16 [4] [see Eq. (1a)]. The actual geometric and material properties discussed in the previous sections were used in the calculation. The correlation of the actual (M_a) and predicted nominal strengths ($M_{n\text{-}ip}$) is shown in Fig. 18a. By comparing Figs. 14 and 19(a), it can be seen that the proposed method provides more realistic strength predictions for welded joints by considering the bearing mechanism. The mean ratio ($m_R = M_a / M_{n\text{-}ip}$) of the data points in Fig. 18a is 1.86 with a COV of 0.242. A ϕ_w-value of 1.00 was obtained in this case. Since AISC 360-16 uses a ϕ_w-value of 0.75 for fillet weld, the application of the proposed design method, together with $F_{nw} = 0.60F_{EXX}$, provides an acceptable level of safety. However, a more efficient (yet still safe) method to increase design efficiency (i.e. to reduce the m_R-value) is still possible.

(ii) F_{nw} = Eq. (6) based on previous research by Tousignant and Packer [12]. The comparison of the actual and predicted nominal strengths is shown in Fig. 18b, where m_R is 1.33 with a COV of 0.236. A ϕ_w-value of 0.72 was obtained. Comparing to the previous case ($F_{nw} = 0.60F_{EXX}$), this is considerably closer to the AISC 360 target resistance factor for fillet weld (0.75). It should be noted that, since welding can only be carried out around the outer perimeter of the RHS walls, the fillet welds are inherently eccentrically-loaded. In addition, the welds at the footprint of an RHS brace member are generally loaded in a highly non-uniform manner due to variation of stiffness over the chord face. In all, although usually viewed as simplistic in nature, the way in which a fillet weld in a semi-rigid RHS connection transfers load can be rather complex [8-13] and largely depends on the dimensions of the connection elements (i.e. B_b/t_b and t_w/t_b in Eq. (6) based on [12]). Hence, the current AISC 360 nominal weld strength rule ($F_{nw} = 0.60F_{EXX}$) is a remarkable simplification. On the other hand, according to Fig. 18b, Eq. (6) provides a more realistic prediction of the average stress value over the effective width of the RHS branch member (B_e).

(iii) $F_{nw} = (1.3)(0.60F_{EXX})$. To correct for the difference between $F_{nw} = 0.60F_{EXX}$ and Eq. (6) (Figs. 18a and 18b) in a practical manner and to achieve an appropriate resistance factor ($\phi_w \geq 0.75$), it is recommended to simply multiply the joint resistance calculated with $F_{nw} = 0.60F_{EXX}$ by the factor 1.3. The comparison of the actual and predicted nominal strengths is shown in Fig. 18c, where m_R = 1.43 with a COV of 0.242. A ϕ_w-value of 0.77 was obtained, which meets the AISC 360 target resistance factor for fillet welds.

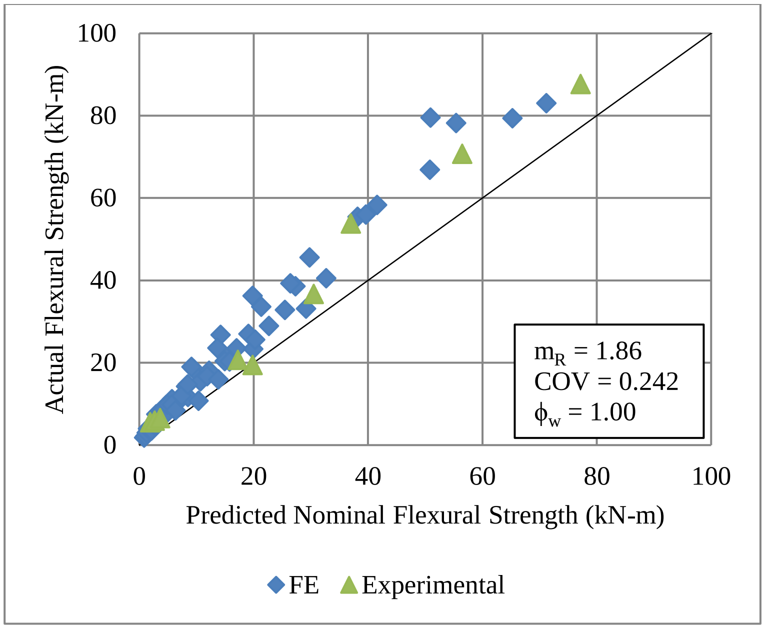

(a) $F_{nw} = 0.60F_{EXX}$ as per AISC 360-16 [4]

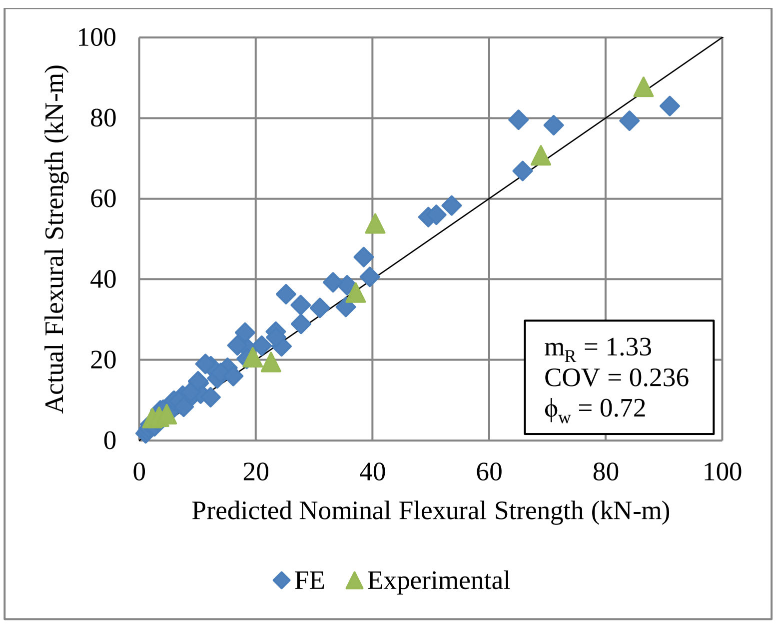

(b) F_{nw} = Eq. (6) based on [12]

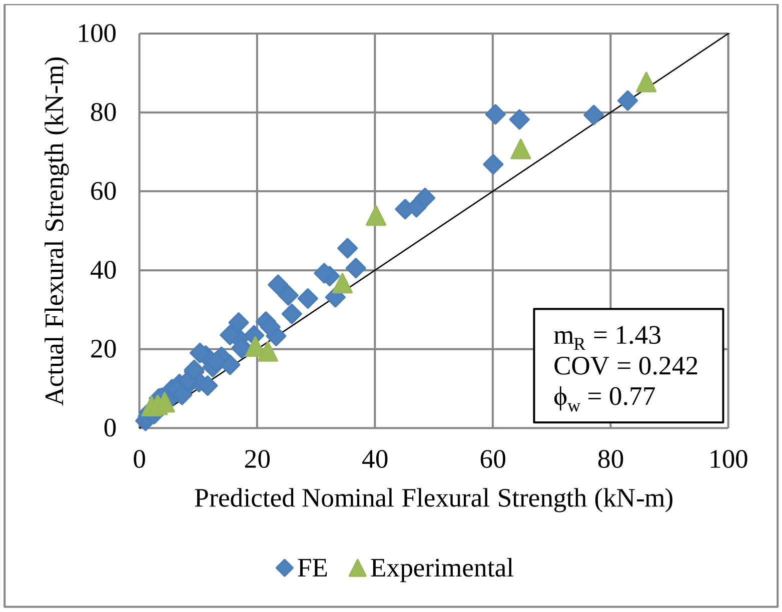

(c) $F_{nw} = (1.3)(0.60F_{EXX})$

Fig. 18. Actual versus predicted nominal flexural strengths using different F_{nw}-values

7.2 Recommendation

Based on the reliability analysis in Section 7.1, it is recommended that the following design provisions be adopted for fillet welds in RHS-to-RHS T-, Y- and X-connections under branch in-plane bending:

$$M_{n-ip} = F_{nw} S_{ip} \tag{13}$$

where:

$$F_{nw} = (1.30)(0.60F_{EXX}) \tag{14}$$

$$S_{ip} = \frac{1}{72}\left[(28t_w + t_b)\left(\frac{H_b}{\sin\theta}\right)^2\right] + \frac{1}{12}\left[(10t_w + t_b)B_e\left(\frac{H_b}{\sin\theta}\right)\right] \tag{15}$$

and:

$$B_e = \left(\frac{10t}{B}\right)\left(\frac{F_y t}{F_{yb} t_b}\right) B_b \leq B_b \tag{16}$$

The above recommendation is subject to the AISC 360-16 [4] Table K.4.2A Limits of Applicability of Table K4.2, plus $B_b/B \leq 0.85$, and applies only to connections with all-around fillet welds.

8. Conclusions

In this paper, effective weld properties in RHS-to-RHS moment T-connections under branch in-plane bending have been investigated. By analysing the data from six experimental tests and 61 numerical FE connection models, it was concluded that the current AISC 360-16 [4] Chapter K formulae for the strength of fillet welds in RHS-to-RHS moment T-connections under branch in-plane bending are over-conservative for the following reasons:

(1) A direct bearing mechanism of load transfer between the branch and the chord on the compression side of the connection is not considered in the S_{ip} formula for in-plane bending given by AISC;

(2) The notwithstanding clause that limits the value of B_e (i.e. "when $\theta > 50^{\circ}$, $B_e / 2$ shall not exceed $B_b / 4$" in Table 1) is excessively conservative for connections under in-plane bending; and

(3) The assumed nominal stress of the fillet-weld metal ($F_{nw} = 0.60F_{EXX}$) is conservative for tension-loaded fillet welds to RHS.

Modifications to the relevant formulae in AISC 360-16 Chapter K were hence proposed. These modifications are shown to provide more accurate predictions of fillet weld strength in RHS-to-RHS moment T-connections under branch in-plane bending and still achieve a reliability index (safety margin) that meets AISC's target value of 4.0 for connections with $\beta \leq 0.85$.

Nomenclature

m_R	mean of ratio: (actual element strength) / (nominal element strength)
t	wall thickness of RHS chord member
t_b	wall thickness of RHS branch member
t_w	weld throat dimension
w	weighting factor
y_t	distance from neutral axis to tension side of connection
B	overall width of RHS chord member
B_b	overall width of RHS branch member
B_e	effective width of RHS branch member
F_{EXX}	ultimate strength of weld metal
F_{nw}	nominal weld strength
F_y	Yield stress of RHS chord material
F_{yb}	Yield stress of RHS branch material
H	overall height of RHS chord member
H_b	overall height of RHS branch member
M_a	actual weld rupture moment
$M_{n\text{-}ip}$	nominal weld strength for in-plane bending
$M_{n\text{-}op}$	nominal weld strength for out-of-plane bending
S_{ip}	effective elastic section modulus of weld for in-plane bending
S_{op}	effective elastic section modulus of weld for out-of-plane bending
α	separation factor = 0.55
β	branch-to-chord width ratio
β^+	safety index = 4.0
γ	half width-to-thickness ratio for chord

568	ε	engineering strain
569	ε_{ef}	equivalent strain fracture criterion
570	ε_T	true strain
571	ε_T'	true strain at the start of necking
572	σ	engineering stress
573	σ_c	maximum stress on compressive side of connection under in-plane bending
574	σ_T	true stress
575	σ_T'	true stress at the start of necking
576	τ	branch-to-chord thickness ratio
577	ϕ_w	resistance factor for welded joint
578	$\phi_{\beta+}$	adjustment factor for β^+
579	θ	branch inclination angle

Acknowledgement

The authors gratefully acknowledge financial support from the Natural Sciences and Engineering Research Council of Canada (NSERC).

References

[1] J.A. Packer, J. Wardenier, X.L. Zhao, G.J. van der Vegte, Y. Kurobane, Design Guide for Rectangular Hollow Section (RHS) Joints under Predominantly Static Loading, CIDECT Design Guide No. 3, 2nd ed CIDECT, Geneva, Switzerland, 2009.

[2] J.A. Packer, D.R. Sherman, M. Lecce, Design Guide No. 24, Hollow Structural Section Connections. American Institute of Steel Construction, Chicago, IL, USA, 2010.

[3] ISO (International Organization for Standardization), ISO 14346:2013 (E), Static design procedure for welded hollow section joints – Recommendations, Geneva, Switzerland, 2013.

[4] American Institute of Steel Construction (AISC), ANSI/AISC 360-16, Specification for Structural Steel Buildings. Chicago, IL, USA, 2016.

[5] G.S. Frater, J.A. Packer, Weldment design for RHS truss connections. I: applications, J. Struct. Eng. ASCE 118(10) (1992) 2784–2803.

[6] G.S. Frater, J.A. Packer, Weldment design for RHS truss connections. II: experimentation, J. Struct. Eng. ASCE 118(10) (1992) 2804–2820.

[7] J.A. Packer, C.E. Cassidy, Effective weld length for HSS T, Y and X connections, J. Struct. Eng. ASCE 121(10) (1995) 1402-1408.

[8] J.A. Packer, M. Sun, Weld design for rectangular HSS connections, Eng. J. AISC 48(1) (2011) 31-48.

[9] M.R. McFadden, M. Sun, J.A. Packer, Weld design and fabrication for RHS connections, Steel Construction – Design and Research 6(1) (2013) 5-10.

[10] J.A. Packer, M. Sun, K. Tousignant, Experimental evaluation of design procedures for fillet welds to hollow structural sections, J. Struct. Eng. ASCE 142 (5) (2016) 04016007-1 – 04016007-12.

[11] K. Tousignant, J.A. Packer, Weld effective lengths for rectangular HSS overlapped K-connections, Eng. J. AISC 52(4) 2015 259–282.

[12] K. Tousignant, J.A. Packer, Numerical investigation of fillet welds in HSS-to-rigid end-plate connections, J. Struct. Eng. ASCE 143(12) (2017) 04017165-1–04017165-16.

[13] M.R. McFadden, J.A. Packer, Effective weld properties for hollow structural section T-connections under branch in-plane bending, Eng. J. AISC 51(4) (2014) 247-266.

[14] K. Tousignant, J.A. Packer, Fillet weld effective lengths in CHS X connections. I: Experimentation, J. Constr. Steel Res. 138 (2017) 420-431.

[15] K. Tousignant, J.A. Packer, Fillet weld effective lengths in CHS X connections. II: Finite element modeling, parametric study and design. J. Constr. Steel Res. 141 (2018) 77-90.

[16] K. Tousignant, J.A. Packer, Fillet welds around circular hollow sections, Welding in the World IIW (2019) In Press.

[17] American Institute of Steel Construction (AISC), ANSI/AISC 360-10, Specification for Structural Steel Buildings. Chicago, IL, USA, 2010.

[18] G. Davies, J.A. Packer, Predicting the strength of branch plate - RHS connections for punching shear, Can. J. Civ. Eng. 9(3) (1982) 458-467.

[19] Dassault Systèmes, ABAQUS Version 6.14 [Computer software]. Dassault Systèmes, Providence, RI, USA, 2014.

[20] G. Martinez-Saucedo, J.A. Packer, S. Willibald, Parametric finite element study of slotted end connections to circular hollow sections, Eng. Struct. 28(14) (2006) 1956-1971.

[21] A.P. Voth, J.A. Packer, Branch plate-to-circular hollow structural section connections. I: experimental investigation and finite-element modeling, J. Struct. Eng. ASCE 138 (8) (2012) 995-1006.

[22] Y. Ling, Uniaxial true stress-strain after necking, AMP J. Technol. 5 (1) (1996) 37-48.

[23] J. Aronofsky, Evaluation of stress distribution in the symmetrical neck of flat tensile bars, J. Appl. Mech. 3 (1951) 75-84.

[24] American Institute of Steel Construction (AISC), Steel Construction Manual, 15th ed, 2017 Chicago, IL, USA.

[25] B.L. Mehrotra, A.K. Govil, Shear lag analysis of rectangular full-width tube connections. J. Struct. Div. ASCE 98(1) (1972) 287-305.

[26] M.K. Ravindra, T.V. Galambos, Load and resistance factor design for steel, J. Struct. Div. ASCE 104(9) (1978) 1337-1353.

[27] J.W. Fisher, T.V. Galambos, G.L. Kulak, M.K. Ravindra, Load and resistance factor design criteria for connectors, J. Struct. Div. ASCE 104(9) (1978) 1427–1441.

[28] C.R. Franchuk, R.G. Driver, G.Y. Grondin, Block shear failure of coped steel beams, Proc. Annual Conf. of the Canadian Society for Civil Engineering, Montreal, 5-8 June 2002, pp. 1000-1009.